



1 **Study of the footprints of short-term variation in XCO₂ observed by TCCON**
2 **sites using NIES and FLEXPART atmospheric transport models**

3 **D.A. Belikov^{1,2,3}, S. Maksyutov¹, A. Ganshin^{3,4}, R. Zhuravlev^{3,4}, N.M. Deutscher^{5,6},**
4 **D. Wunch⁷, D.G. Feist⁸, I. Morino¹, R. J. Parker⁹, K. Strong¹⁰, Y. Yoshida¹, A. Bril¹¹,**
5 **S. Oshchepkov¹¹, H.Boesch⁹, M. K. Dubey¹², D. Griffith⁵, W. Hewson⁹, R. Kivi¹³, J.**
6 **Mendonca¹⁰, J. Notholt⁶, M. Schneider¹⁴, R. Sussmann¹⁵, V.A. Velazco⁵, and S. Aoki¹⁶**

7 [1]{National Institute for Environmental Studies, Tsukuba, Japan}

8 [2]{National Institute of Polar Research, Tokyo, Japan}

9 [3]{Tomsk State University, Tomsk, Russia}

10 [4]{Central Aerological Observatory, Dolgoprudny, Russia}

11 [5]{Centre for Atmospheric Chemistry, School of Chemistry, University of Wollongong,
12 Wollongong, NSW, Australia}

13 [6]{Institute of Environmental Physics, University of Bremen, Bremen, Germany}

14 [7]{California Institute of Technology, Pasadena, CA, USA}

15 [8]{Max Planck Institute for Biogeochemistry, Jena, Germany}

16 [9]{Earth Observation Science, University of Leicester, Leicester, UK}

17 [10]{Department of Physics, University of Toronto, Toronto, ON, Canada}

18 [11]{Institute of Physics of the National Academy of Sciences, Minsk, Belarus}

19 [12]{Earth System Observations, Los Alamos National Laboratory, Los Alamos, New Mexico}

20 [13]{Finnish Meteorological Institute, Sodankylä, Finland}

21 [14]{Agencia Estatal de Meteorología (AEMET), CIAI, Santa Cruz de Tenerife, Spain}

22 [15]{Karlsruhe Institute of Technology, IMK-IFU, Garmisch-Partenkirchen, Germany}

23 [16]{Tohoku University, Sendai, Japan}

24

25 Correspondence to: D. A. Belikov (dmitry.belikov@nies.go.jp)

26



1 **Abstract**

2 The Total Carbon Column Observing Network (TCCON) is a network of ground-based
3 Fourier Transform Spectrometers (FTS) that record near-infrared (NIR) spectra of the Sun.
4 From these spectra, accurate and precise observations of CO₂ column-averaged dry-air mole
5 fraction (denoted XCO₂) are retrieved. TCCON FTS observations have previously been used to
6 validate satellite estimations of XCO₂; however, our knowledge of the short-term spatial and
7 temporal variations in XCO₂ surrounding the TCCON sites is limited.

8 In this work, we use the National Institute for Environmental Studies (NIES) Eulerian
9 three-dimensional transport model and the FLEXPART (FLEXible PARTicle) Lagrangian
10 Particle Dispersion Model (LPDM) to determine the footprints of short-term variations in
11 XCO₂ observed by operational, past, future, and possible TCCON sites. We propose a footprint-
12 based method for the collocation of satellite and TCCON XCO₂ observations, and estimate the
13 performance of the method using the NIES model and five GOSAT XCO₂ product datasets.
14 Comparison of the proposed approach with a standard geographic method shows higher
15 number of collocation points and average bias reduction up to 0.15 ppm for a subset of 16
16 stations for the period from January 2010 to January 2014. Case studies of the Darwin and La
17 Réunion sites reveal that when the footprint area is rather curved, non-uniform and
18 significantly different from a geographical rectangular area, the differences between these
19 approaches are more noticeable. This emphasizes that the collocation is sensitive to local
20 meteorological conditions and flux distributions.

21

22 **Keywords:** XCO₂, TCCON, GOSAT, atmospheric transport

23



1 1. Introduction

2 Satellite observations of the column-averaged dry-air mole fraction of CO₂ (XCO₂) have
3 the potential to significantly advance our knowledge of carbon dioxide (CO₂) distributions
4 globally and provide new information on regional CO₂ sources and sinks. Observations of
5 XCO₂ are available from space-based instruments such as the SCanning Imaging Absorption
6 SpectroMeter for Atmospheric CHartographyY (SCIAMACHY; Bovensmann et al., 1999), the
7 Greenhouse gases Observing Satellite (GOSAT; Kuze et al., 2009, 2016; Yokota et al., 2009),
8 and the Orbiting Carbon Observatory-2 (OCO-2; Crisp et al., 2004). These satellites provide
9 unprecedented spatial coverage of the variability in XCO₂ around the world, with the
10 exception of polar regions and areas with dense clouds. These observations are, however,
11 limited by the orbit of the satellites, which typically measure in the local afternoon.

12 Ground-based Fourier Transform Spectrometer (FTS) observations available from the
13 Total Carbon Column Observing Network (TCCON) (Wunch et al., 2011) provide dense
14 temporal resolution and are more precise and accurate than space-based instruments.
15 However, the number of ground-based FTS sites is limited, with just 23 operational sites and
16 several approved for the future. These sites are sparsely distributed, and Siberia, Africa, South
17 America, and the oceans from middle to high latitudes are poorly covered. Despite this
18 limitation, FTS observations are used to validate satellite retrievals in order to assess bias,
19 variability, and other key parameters (e.g., Wunch et al., 2011; Lindqvist et al., 2015).

20 The spatial and temporal coverage of satellite observations over TCCON sites is sparse
21 due to cloud and aerosol filters, retrieval selection criteria, and post-retrieval data quality
22 filters. To obtain satellite observation data with small uncertainties it is necessary to apply a
23 collocation method for aggregating neighboring soundings. Currently available methods for
24 XCO₂ collocation include geographical (e.g., Cogan et al., 2012; Inoue et al., 2013; Reuter et al.,
25 2013), T700 (it implies that the air with the same history of transport derived from the 700
26 hPa potential temperature has the same XCO₂; Wunch et al., 2011), model-based (Guerlet et
27 al., 2013), and geostatistical approaches (Nguyen et al., 2014).

28 In the geographical collocation method a spatial region around a TCCON site is selected
29 together with a temporal window. Inoue et al. (2013) used daily mean observations within a
30 10° × 10° area, Reuter et al. (2013) selected the monthly median of all observations within a
31 10° × 10° area, and Cogan et al. (2012) implemented narrower limits, using a two-hour mean
32 period within a ±5° × ±5° area.

33 To increase the number of soundings, the spatial region may be expanded and additional



1 selection criteria imposed. In the T700 collocation method proposed by Wunch et al. (2011),
2 all observations within $\pm 30^\circ$ longitude, $\pm 10^\circ$ latitude, ± 5 days, and ± 2 K of the selected TCCON
3 location are employed.

4 The model-based method proposed by Oshchepkov et al. (2012) and improved by
5 Guerlet et al. (2013) uses daily mean values within 0.5 ppm of the 3 day-averaged model XCO₂
6 values and located within $\pm 25^\circ$ longitude and $\pm 7.5^\circ$ latitude of a TCCON site.

7 Nguyen et al. (2014) developed a geostatistical collocation methodology that selects
8 observations using a “distance” function, which is a modified Euclidian distance in terms of
9 latitude, longitude, time, and mid-tropospheric temperature at 700 hPa.

10 Bremen, Garmisch, Four Corners, JPL, and Izaña are influenced by local effects or
11 complex terrain and are not included in averages (Kulawik ATM 2016). Limitations of the
12 techinks !!!

13 The majority of collocation methods described above have a common disadvantage; i.e.,
14 they work with a rectangular spatial domain, which is convenient for technical handling but
15 does not reflect the impact of surface sources or sinks of CO₂ and the local meteorology in the
16 area of interest. The spatial domains in collocations should take into account these features to
17 ensure that only appropriate observations are selected. Keppel-Aleks et al. (2011, 2012)
18 showed that the largest gradient in XCO₂ is formed mainly by the north-south flux
19 distribution, with variations in XCO₂ caused mainly by large-scale advection. TCCON and
20 satellite XCO₂ observations have pronounced temporal variability and are thus important in
21 studies of short-term variations in XCO₂.

22 In this paper we study short-term variations in XCO₂ observed at TCCON sites. Although
23 the XCO₂ is derived from column-averaged concentrations of CO₂, XCO₂ observations are most
24 sensitive to near-surface fluxes. The XCO₂ variations are thus related to changes in the CO₂
25 mole fraction occurring near the surface surrounding the TCCON sites (hereafter known as
26 the footprints of the TCCON sites).

27 The remainder of this paper is organized as follows: an overview of the method for
28 estimating the footprints of TCCON sites is presented in Section 2. The results of the footprint
29 estimation and a new method for collocation are presented and discussed in Sections 3,4, and
30 the conclusions are given in Section 5.



1 2. Method

2 To estimate the footprints of TCCON sites we used forward simulations employing the
3 NIES Eulerian three-dimensional transport model (TM) and backward trajectory tracking
4 using the FLEXPART LPDM model. NIES TM CO₂ concentrations sampled at 1 km above
5 ground at 13:00 local time were used to initialize backward tracer simulations with the
6 FLEXPART model. FLEXPART, like other Lagrangian Particle Dispersion Models (LPDMs),
7 considers atmospheric tracers as a discrete phase and tracks the pathway of each individual
8 particle (Stohl et al., 2009). The level of 1 km above ground typically corresponds to the top of
9 the daytime planetary boundary layer (PBL). The PBL is the lowest part of the atmosphere
10 and its behavior is directly influenced by its contact with the planetary surface. Turbulence
11 causes intensive vertical mixing of the air within the PBL, so CO₂ released from the surface is
12 roughly uniformly distributed throughout the column of air in the PBL at local noon, when the
13 maximum extent of vertical mixing occurs. The selected sampling time is also favorable for
14 minimizing errors in the initial CO₂ concentration calculated by NIES TM, as this type of
15 chemical transport model has proved to be successful in resolving the diurnal vertical profiles
16 of tracers (Belikov et al., 2013a).

17 The NIES model has previously been used to study the seasonal and inter-annual
18 variability in CO₂. Belikov et al. (2013b) reported that the NIES model is able to successfully
19 reproduce the vertical profile of CO₂ as well as the seasonal and inter-annual variability in
20 XCO₂. A comparison of modeled output with TCCON observations (Belikov et al., 2013b)
21 revealed model biases of ±0.2% for XCO₂; on this basis we assume that the NIES TM is able to
22 successfully reproduce the vertical profile of CO₂ at the locations of TCCON sites.

23 The key features of the NIES TM are as follows: a reduced horizontal latitude–longitude
24 grid with a spatial resolution of 2.5° × 2.5° near the equator (Belikov et al., 2011); a vertical
25 flexible hybrid sigma–isentropic (σ – θ) grid with 32 levels up to the level of 5 hPa (Belikov et
26 al., 2013b); separate parameterization of the turbulent diffusivity in the PBL and free
27 troposphere (provided by the European Centre for Medium-Range Weather Forecasts
28 (ECMWF) ERA-Interim reanalysis); and a modified Kuo-type parameterization scheme for
29 cumulus convection (Belikov et al., 2013a). The NIES TM was run using fluxes obtained with
30 the GELCA-EOF (Global Eulerian-Lagrangian Coupled Atmospheric model with Empirical
31 Orthogonal Function) inverse modeling scheme (Zhuravlev et al., 2013). A priori fluxes
32 consist of four types: 1) the Open source Data Inventory of Anthropogenic CO₂ (ODIAC) (Oda
33 et al., 2011) and the Carbon Dioxide Information Analysis Center's (CDIAC) (Andres et al.,



1 2011) anthropogenic fluxes; 2) the Vegetation Integrative Simulator for Trace gases (VISIT)
2 (Ito, 2010) biosphere fluxes; 3) the Offline ocean Tracer Transport Model (OTTM) (Valsala et
3 al., 2013) oceanic fluxes; and 4) the Global Fire Emissions Database (GFED) (Van der Werf et
4 al., 2010) biomass burning emissions. The NIES and FLEXPART models are driven by the
5 Japanese Meteorological Agency Climate Data Assimilation System (JCDAS) datasets (Onogi et
6 al., 2007).

7 Variations in TCCON XCO₂ are influenced by a large spatial footprint. Keppel-Aleks et al.
8 (2012) presented a robust relationship between weekly and monthly aggregated total column
9 CO₂ and local net ecosystem exchange, while column drawdown has only a weak correlation
10 with the regional flux on daily timescales. The maximum trajectory duration for the model
11 was therefore set to one week. The model was run to analyze TCCON site footprints for a 14-
12 month period from January 2010 to February 2011. The FLEXPART model was then used to
13 identify the areas in which TCCON soundings are most sensitive to variations on a short-term
14 scale.



1 **3. Results**

2 **3.1. Sensitivity of TCCON site footprints**

3 We analyzed two groups of TCCON sites: operational sites (Table 1; Figs. 1 and 2) and
4 past, future, and possible sites (Table 2; Fig. 3). We included Arrival Heights (Antarctica) and
5 Yekaterinburg (Russia) in the second group, though the status of these monitoring stations is
6 unclear. The footprint estimation is restricted to the summer season for high-latitude sites
7 (Arrival Heights, Eureka, Ny Ålesund, Poker Flat, and Sodankylä), due to limitations relating to
8 the solar zenith angle.

9 **3.1.1. Operational sites**

10 ***North America***

11 The five active American sites are located in the US and Canada, so they are sensitive to
12 the western and central part of North America, the northern part of Canada and Greenland,
13 and the eastern part of the Pacific Ocean. There are no TCCON sites in Alaska or on the east
14 coast of North America, which is a region of intense anthropogenic activity (Fig. 1).

15 ***European sites***

16 The European region contains eight operational sites (Fig. 2). We also include Izaña,
17 which does not belong to this region but is located very close to it. This region has a good
18 spatial coverage of operational TCCON sites; however, most sites are located near the coast
19 and are thus very sensitive to the Atlantic and Arctic oceans. The maximum footprint
20 sensitivity occurs in western Europe where there is a high density of operational TCCON sites;
21 five sites (Bremen, Garmisch, Karlsruhe, Orléans, and Paris) are concentrated within a small
22 area. The sensitivity decreases quite rapidly towards the east and south, and only parts of
23 eastern Europe and north Africa are covered.

24 ***Asia***

25 The footprints of Asian sites mainly span countries bordering the Sea of Japan; i.e., Japan,
26 Korea, the Russian Far East, and east China. These sites are also able to capture signals from
27 Mongolia, eastern Siberia, and Southeast Asia. Although the coverage of these sites is
28 relatively small, the main industrial centers in the region are included.

29 ***Australia and New Zealand***

30 The footprint sensitivity of TCCON sites in this region covers almost all of Australia.
31 Chevallier et al. (2011) shows TCCON data could constrain flux estimates over Australia



1 equally well as the existing in situ measurements. Our footprint estimations are, however,
2 more sensitive to the ocean regions between Australia and New Zealand as well as adjacent
3 coastal areas.

4 ***Oceanic sites: Ascension Island and La Réunion Island***

5 Ascension Island is in the Trade Wind belt of the tropical Atlantic, ideally located to
6 measure the South Atlantic marine boundary layer. The South East Trade Winds, which are
7 almost invariant and are derived from the deep South Atlantic Ocean with little contact with
8 Africa. Surface measurements of CO₂ at Ascension Island are used as a background (Gatti et al.,
9 2010). However, above the Trade Wind Inversion (TWI), at about 1200–2000 m above sea
10 level, the air masses are very different, coming dominantly from tropical Africa and
11 occasionally South America (Swap et al., 1996). The FLEXPART simulation with tracers
12 released at an altitude of 3000 m detected some hotspots in Africa (Fig. 1b). The study of
13 biomass burning in Africa is essential, but lies outside of the scope of this paper.

14 La Réunion island situated in the Indian Ocean at about 800 km east of Madagascar. For
15 this site the seasonal trend of wind mainly remains in the easterly sector, so the footprint
16 covers mainly ocean regions. La Réunion site is further discussed in Section 4.3.2.

17 **3.1.2. Past, future, and possible TCCON sites**

18 The footprints of past, future, and possible TCCON sites are presented in Fig. 3. The
19 Oxfordshire site enhances the sensitivity of the region, which is already well covered by
20 existing TCCON sites in Europe. The East Trout Lake, Four Corners, and Poker Flat sites fill
21 sensitivity gaps in the Canadian Boreal forest, the southwestern US, northern Mexico, and
22 Alaska. Nevertheless, there are no TCCON sites near the Atlantic coast of North America,
23 which is a key region of interest.

24 In South America, the Manaus site (briefly in operation during 2014 and will operate
25 after reconstruction) was ideally located in central Amazonia. However, meteorological
26 conditions meant that a signal was only detected in a very narrow section towards the east.
27 Observations at this site are more sensitive to anthropogenic activity on the Atlantic coast of
28 South America, compared with the surrounding Amazonian biosphere. Additional use of CO
29 observations will be necessary to isolate the Net Primary Production signal in Central
30 Amazonia (Keppel-Aleks et al., 2012). Another site in this region is Paramaribo located in
31 Suriname which is part of Caribbean South America. The footprint of the Paramaribo site is
32 narrowly focused towards the Atlantic Ocean due to site location and meteorological



1 conditions as stated above.

2 Burgos in the northern Philippines extends the Asian footprint southward. The location
3 of the Yekaterinburg site is ideal, as it quite evenly covers a large area of western Russia. The
4 site reduces the gap between the European and Asian TCCON domains. The Arrival Heights
5 site is located on the Antarctic coast and currently cannot be used for satellite data validation.
6 Given the air circulation near the South Pole, this site can be useful for measuring the
7 background value of XCO₂.

8 In general, the operational stations cover some regions well (North America, Europe, the
9 Far East, Southeast Asia, Australia, and New Zealand), and the planned sites will improve this
10 coverage. However, on a global scale there are major gaps that highlight the difficulty in
11 generalizing the available data along latitude for bias correction.

12 The short-term variations in CO₂ in the near surface and free troposphere (<3000 m)
13 have the same form, but different intensity (Fig. 1b), as a smaller number of tracers from the
14 middle troposphere reached the surface during the simulation time.

15 **3.2. Seasonal variability in footprints**

16 Some TCCON stations have strong seasonal variations in their footprint due to changes
17 in wind direction; i.e., Białystok, Darwin, Izaña, Park Falls, and Tsukuba (Fig. 4). For other
18 sites (e.g., Ascension and Manaus) the weather conditions are less variable throughout the
19 year. The depth of the PBL changes with season and is thus an important factor that influences
20 the footprint. In winter the PBL lowers, causing less vertical mixing and enhancing horizontal
21 tracer transport; this leads to a wider spatial coverage of the footprints.

22 **4. Applying the model-derived footprints to the colocation of XCO₂**

23 In the next two sections we assess the performance of the footprint-based method of
24 collocating TCCON XCO₂ against the NIES model and GOSAT product datasets. The colocation
25 domain size for each site is determined by sensitivity values (ppm (μmol (m²s)⁻¹)⁻¹) with the
26 limits of log₁₀(x) equal to -0.5, -1.0, -1.5, and -2.0 (cases C1-C4). These sensitivity values
27 were selected to approximately correspond to the domain sizes in standard geographical
28 colocation techniques, which have rectangular dimensions of 2.5° × 2.5°, ±5.0° × ±5.0°, ±5.0° ×
29 ±10.0°, and ±7.5° × ±22.5° (cases C5-C8). Only coincident observations were used, and
30 observations with differences of ≥3 ppm were discarded from the comparison. Considered
31 period for comparison is January 2010 and January 2014.



1 TCCON observations were used from 16 sites: Białystok, Caltech, Darwin, Eureka,
2 Garmisch, Izaña, Karlsruhe, Lamont, Lauder (125HR), Orléans, Park Falls, La Réunion Island,
3 Saga, Sodankylä, Tsukuba (125HR), and Wollongong. These observations were obtained from
4 the 2014 release of TCCON data (“GGG2014”), available from the TCCON Data Archive
5 (<http://tccon.ornl.gov>).

6 **4.1. Colocation of XCO₂ from TCCON and the NIES model**

7 The TCCON and NIES TM datasets are initially compared using a geographical colocation
8 of $2.5^\circ \times 2.5^\circ$ that corresponds to selecting the nearest NIES TM cell (Table 3). The resolution
9 of the model grid is rather coarse, so we observe that the results depend mainly on the size of
10 the colocation area but not on the form. With increasing size of the colocation area the
11 correlation between XCO₂ from TCCON and NIES TM slightly increases from 0.96 to 0.97 and
12 the standard deviation decreases from 1.1 to 0.96 ppm. This is due to an increase in the
13 number of observations, which results in a larger average bias.

14 For Darwin, Eureka, Izaña, Lauder, La Réunion, Sodankylä, and Wollongong, the
15 residuals between the datasets are small and similar for all methods (see Fig. 5a for Darwin;
16 cases C1, C4, C5, and C8). Here, XCO₂ is under the influence of global long-term variations that
17 are included in the NIES TM. The low sensitivity of the model to local sources does not cause a
18 significant difference between the colocation methods. For the second group (non-operational
19 sites), local sources are essential and even coarse-grid models can capture their signal. As a
20 result, the shape of the colocation area is important (see Fig. 5b for Garmisch; cases C1, C4, C5,
21 and C8).

22 **4.2. Colocation of XCO₂ from TCCON and GOSAT products**

23 A comparison of colocation methods was performed for five GOSAT XCO₂ products: NIES
24 v02.11 (Yoshida et al., 2013) and PPDF-S v02.11 from the NIES, Japan (Oshchepkov et al.,
25 2013); ACOS B3.4 from the NASA Atmospheric CO₂ Observations from Space (ACOS) team
26 (O’Dell et al., 2012); RemoTeC v2.11 from the Netherlands Institute for Space
27 Research/Karlsruhe Institute of Technology, Germany (Butz et al., 2011; Guerlet et al., 2013);
28 and UoL-FP v4 from the University of Leicester, UK (Boesch et al., 2011; Cogan et al., 2012).

29 The results of the comparison of eight colocation methods employed for the five GOSAT
30 XCO₂ products are presented in Tables 4–8. Only coincident observations were used, and
31 observations with differences of ≥ 3 ppm were discarded from the comparison. The number of
32 observations selected for colocation between the methods with the smallest areas (C1 and C5)



1 and largest areas (C4 and C8) differs by about 5 times. There is, however, no clear dependence
2 of the collocation efficiency on the number of observations. The correlation coefficient and
3 standard deviation are within 0.81–0.93 ppm and 1.02–1.22 ppm, respectively, regardless of
4 the method used. Mean bias values are within 0.50–0.87 ppm, with the footprint method
5 typically having a slightly lower bias by 0.02–0.15 ppm and higher number of collocations. For
6 individual stations, these statistics may lie slightly outside the specified ranges.

7 **4.3. Case study**

8 In this section we demonstrate the developed collocation method for GOSAT
9 observations over the Darwin and La Réunion Island TCCON sites.

10 **4.3.1. Darwin site**

11 Darwin lies in the Northern Territory, Australia, which has two distinctive climate zones.
12 The northern zone, including Darwin, has distinct wet and dry seasons and the average
13 maximum temperature is remarkably similar all year round. The dry season (May to
14 September), the build-up season (high humidity, but little rain: October to December) and the
15 wet season associated with tropical cyclones and monsoon rains (December to April). The
16 southern zone is mainly desert with a semi-arid climate and little rain. To the north of Darwin,
17 the territory is bordered by the Timor Sea, the Arafura Sea, and the Gulf of Carpentaria. The
18 Northern Territory therefore has a pronounced seasonal variability that affects the spatial and
19 temporal distribution of CO₂ and thus the footprint (Figs 4 and 6a).

20 Figures 6b and 6c show the locations of GOSAT observations selected using a
21 geographical method within an area of $\pm 7.5^\circ \times \pm 22.5^\circ$ and a footprint-based method with the
22 limit $\log_{10}(x) = -2.0$. Sizes of selected collocation areas (C4 and C8 methods) are close to ones
23 used in others works (Wunch et al., 2011, Guerlet et al., 2013, Inoue et al. 2013, Reuter et al.
24 2013, Nguyen et al., 2014).

25 For ACOS, NIES, and RemoTeC GOSAT products the distributions of XCO₂ datasets for the
26 Darwin site are similar and cover an area to the west of Darwin, including ground-based
27 observations from central Australia (Fig. 6c). The comparison of collocation methods shows
28 the footprint-based method (C4) outperforms the geographical method (C8) for these three
29 GOSAT products (Fig. 7), with approximately 3 times as many observations.

30 Although currently the UoL GOSAT XCO₂ version 6 includes ocean-glint observations, in
31 this study we use slightly outdated the UoL-FP GOSAT product v4, which has only overland



1 points. In this case the difference between colocations subsets is the observations towards the
2 south over land, which provide a similar distribution as the ACOS product, but without marine
3 observations (Fig. 6b and Fig. 6c). These differences in the covered areas have a significant
4 negative effect on the result (Fig. 7). From that it can be concluded that XCO₂ patterns towards
5 the south over land are rather different from those around Darwin, the sun-glint observation
6 over the ocean are important and must be included into analysis. Thus, XCO₂ at the Darwin
7 site is under the influence of the three different fluxes coming from surrounding land area,
8 central part of Australia and oceanic regions. The oceanic observation over the Coral sea is
9 quite important, though substantially removed from the station.

10 **4.3.2. La Réunion site**

11 La Réunion is a small island east of Madagascar surrounded by the Indian Ocean. The
12 nearest land territory to La Réunion is Mauritius, located ~175 km to the northwest. The
13 meteorological conditions in the region mean that the footprint of the La Réunion site mostly
14 covers a large area of ocean to the southeast of the island and a small area of northern
15 Madagascar (Fig. 8).

16 The geographical colocation method does not take into account local conditions.
17 Therefore, despite the fact that the site is predominantly oceanic, the geographical method
18 includes observations made over land in Madagascar and the southeast coast of Africa (Fig.
19 8b). In contrast, the footprint method takes into account the local meteorology, so
20 observations are predominantly taken from the ocean (Fig. 8c). Since the UoL-FP dataset has
21 no observations over the sea, the observations for this dataset are located only over
22 Madagascar (Fig. 9).

23 Unlike Darwin, La Réunion receives clean air from the ocean and thus has very little CO₂
24 variation. The selection of areas for colocation therefore did not reveal any significant
25 advantages of the footprint-based method, with the exception of a slightly smaller bias for the
26 NIES and RemoTec products (Fig. 10). The comparison of the UoL-FP product for method C4
27 and method C8 shows that the XCO₂ cycles over Madagascar and the eastern coast of Africa
28 are quite different (Fig. 10). This highlights that the exclusion of marine observations leads to
29 poor results over marine-based TCCON sites.

30 A comparison of TCCON data and NIES model results for Darwin and La Réunion shows
31 that XCO₂ for these sites is controlled mainly by large-scale changes. However, analysis of
32 GOSAT products emphasizes that the influence of local sources is also important. The



1 geographical method of collocation assumes a fairly even distribution of GOSAT observations
2 near TCCON sites, while the calculated footprints have strongly curved shapes and an uneven
3 distribution. We therefore expect the proposed footprint method to be useful for other sites
4 with rather curved and non-uniform footprints, such as the Ascension Island and Manaus
5 sites.

6 **5. Summary**

7 We have developed a method for assessing the footprints of short-term XCO₂ variations
8 observed by TCCON ground-based FTS sites. The method is based on one-week FLEXPART
9 backward trajectory simulations that are initiated at an altitude of 1 km (the upper border of
10 the PBL) in the afternoon using the vertical CO₂ distribution calculated by the NIES transport
11 model.

12 We applied this method to estimate footprints of the operational, past, future, and
13 possible TCCON sites, and revealed some basic patterns. Most sites located near coastal
14 regions are strongly influenced by ocean regions; thus, there is a large seasonal variability in
15 footprints for Białystok, Darwin, Izaña, Park Falls, and Tsukuba. The Ascension Island,
16 Manaus, and La Réunion sites have very narrow footprints that show small seasonal
17 variations.

18 We proposed the footprint-based method for the collocation of satellite observations
19 with TCCON sites, and assessed the performance of the method using the NIES model and
20 GOSAT product datasets. The collocation footprint area is determined by yearly averaged
21 sensitivity values with limits of $\log_{10}(x)$ equals -0.5 , -1.0 , -1.5 and -2.0 . These were selected
22 to approximately correspond to the areas of standard geographical collocation techniques that
23 have rectangular shapes of $2.5^\circ \times 2.5^\circ$, $\pm 5.0^\circ \times \pm 5.0^\circ$, $\pm 5.0^\circ \times \pm 10.0^\circ$, and $\pm 7.5^\circ \times \pm 22.5^\circ$,
24 respectively. Comparison of the proposed method with the geographical method showed
25 similar but smaller biases for a subset of 16 stations for the period from January 2009 to
26 January 2014. Case studies of the Darwin and La Réunion TCCON sites revealed that the
27 footprint has a very different collocation area to that of the geographical method, especially
28 near marine coast.

29 This study shows the use of collocation methods similar to geographical, which are based
30 on tracking long-term trends of tracers (i.e. derived from global model calculations) has its
31 limitations and works up to a certain accuracy threshold, after which it is impossible to ignore
32 the influence of local sources. Given that the GOSAT XCO₂ products are sensitive to local



1 sources, proposed footprint method is promising and requires further fine-tuning. The
2 potential for further improvement includes moving from gross annual averaging to more
3 accurate seasonal or monthly averaging. In addition, it is possible to study the sensitivity of
4 XCO₂ observations using adjoint of the global Eulerian–Lagrangian coupled atmospheric
5 transport model (Belikov et al., 2016), which can resolve long-term, synoptic and hourly
6 variation patterns.

7 We believe, however, that the footprint analysis should be considered important in the
8 appraisal of new TCCON sites, along with assessments of the number of cloudless days, the
9 surrounding landscape, and the reflectivity of the Earth's surface.



1 **Acknowledgments**

2 Authors thank Paul Wennberg for insightful discussions and suggestions regarding the
3 manuscript.

4 The JRA-25/JCDAS meteorological datasets used in the simulations were provided by
5 the Japan Meteorological Agency. The computational resources were provided by NIES. This
6 study was performed by order of the Ministry for Education and Science of the Russian
7 Federation No. 5.628.2014/K and was supported by The Tomsk State University Academic D.I.
8 Mendeleev Fund Program in 2014–2015 and by the GRENE Arctic project. TCCON data were
9 obtained from the TCCON Data Archive, hosted by the Carbon Dioxide Information Analysis
10 Center (CDIAC; tcon.ornl.gov).

11 The Ascension Island site has been funded by the Max Planck Society. The Bremen,
12 Białystok, and Orléans TCCON sites are funded by the EU projects InGOS and ICOS-INWIRE,
13 and by the Senate of Bremen. The Darwin and Wollongong TCCON sites are funded by NASA
14 grants NAG5-12247 and NNG05-GD07G, and Australian Research Council grants
15 DP140101552, DP110103118, DP0879468, LE0668470, and LP0562346. We are grateful to
16 the DOE ARM program for technical support at the Darwin TCCON site. Nicholas Deutscher
17 was supported by an Australian Research Council fellowship, DE140100178.

18 The Eureka measurements were made at the Polar Environment Atmospheric Research
19 Laboratory (PEARL) by the Canadian Network for the Detection of Atmospheric Change
20 (CANDAC) led by James R. Drummond, and in part by the Canadian Arctic ACE Validation
21 Campaigns led by Kaley A. Walker. They were supported by the AIF/NSRIT, CFI, CFCAS, CSA,
22 EC, GOC-IPY, NSERC, NSTP, OIT, ORF, and PCSP.

23 The University of Leicester data were obtained with funding from the UK National
24 Centre for Earth Observation and the ESA GHG-CCI project, using the ALICE High Performance
25 Computing Facility at the University of Leicester. R. Parker was funded by an ESA Living
26 Planet Fellowship.



1 **References**

- 2 Andres, R. J., Gregg, J. S., Losey, L., Marland, G., and Boden, T.: Monthly, global emissions of
3 carbon dioxide from fossil fuel consumption, *Tellus*, 63B, 309–327, 2011.
- 4 Belikov, D., Maksyutov, S., Miyasaka, T., Saeki, T., Zhuravlev, R., and Kiryushov, B.: Mass-
5 conserving tracer transport modelling on a reduced latitude–longitude grid with NIES-
6 TM, *Geosci. Model Dev.*, 4, 207–222, 2011.
- 7 Belikov, D. A., Maksyutov, S., Krol, M., Fraser, A., Rigby, M., Bian, H., Agusti-Panareda, A.,
8 Bergmann, D., Bousquet, P., Cameron-Smith, P., Chipperfield, M. P., Fortems-
9 Cheiney, A., Gloor, E., Haynes, K., Hess, P., Houweling, S., Kawa, S. R., Law, R. M.,
10 Loh, Z., Meng, L., Palmer, P. I., Patra, P. K., Prinn, R. G., Saito, R., and Wilson, C.: Off-
11 line algorithm for calculation of vertical tracer transport in the troposphere due to
12 deep convection, *Atmos. Chem. Phys.*, 13, 1093–1114, doi:10.5194/acp-13-1093-2013,
13 2013a.
- 14 Belikov, D., Maksyutov, S., Sherlock, V., Aoki, S., Deutscher, N. M., Dohe, S., Griffith, D., Kyro,
15 E., Morino, I., Nakazawa, T., Notholt, J., Rettinger, M., Schneider, M., Sussmann, R.,
16 Toon, G. C., Wennberg, P. O., and Wunch, D.: Simulations of column-average CO₂ and
17 CH₄ using the NIES TM with a hybrid sigma–isentropic (σ – θ) vertical coordinate, *Atmos.*
18 *Chem. Phys.*, 13, 1713–1732, doi:10.5194/acp-13-1713-2013, 2013b.
- 19 Belikov, D. A., Maksyutov, S., Yaremchuk, A., Ganshin, A., Kaminski, T., Blessing, S.,
20 Sasakawa, M., Gomez-Pelaez, A. J., and Starchenko, A.: Adjoint of the global Eulerian–
21 Lagrangian coupled atmospheric transport model (A-GELCA v1.0): development and
22 validation, *Geosci. Model Dev.*, 9, 749–764, doi:10.5194/gmd-9-749-2016, 2016.
- 23 Boesch, H., Baker, D., Connor, B., Crisp, D., and Miller, C.: Global characterization of CO₂
24 column retrievals from shortwave-infrared satellite observations of the Orbiting
25 Carbon Observatory-2 Mission, *Remote Sens.*, 3, 270–304, doi:10.3390/rs3020270,
26 2011.
- 27 Bovensmann, H., Burrows, J. P., Buchwitz, M., Frerick, J., Noël, S., Rozanov, V. V., Chance, K.
28 V., and Goede, A. P. H.: SCIAMACHY: Mission objectives and measurement modes, *J.*
29 *Atmos. Sci.*, 56, 127–150, 1999.
- 30 Butz, A., Guerlet, S., Jacob, D. J., Schepers, D., Galli, A., Aben, I., Frankenberg, C., Hartmann,
31 J.-M., Tran, H., Kuze, A., Keppel-Aleks, G., Toon, G. C., Wunch, D., Wennberg, P. O.,
32 Deutscher, N. M., Griffith, D. W. T., Macatangay, R., Messerschmidt, J., Notholt, J., and
33 Warneke, T.: Toward accurate CO₂ and CH₄ observations from GOSAT, *Geophys. Res.*
34 *Lett.*, 38, 2–7, 2011.
- 35 Chevallier, F., Deutscher, N. M., Conway, T. J., Ciais, P., Ciattaglia, L., Dohe, S., Frohlich, M.,
36 Gomez-Pelaez, A. J., Griffith, D., Hase, F., Haszpra, L., Krummel, P., Kyro, E.,
37 Labuschagne, C., Langenfelds, R., Machida, T., Maignan, F., Matsueda, H., Morino, I.,
38 Notholt, J., Ramonet, M., Sawa, Y., Schmidt, M., Sherlock, V., Steele, P., Strong, K.,
39 Sussmann, R., Wennberg, P., Wofsy, S., Worthy, D., Wunch, D., and Zimnoch, M.:
40 Global CO₂ fluxes inferred from surface air-sample measurements and from TCCON
41 retrievals of the CO₂ total column, *Geophys. Res. Lett.*, 38, L24810,
42 doi:10.1029/2011GL049899, 2011



- 1 Cogan, A. J., Boesch, H., Parker, R. J., Feng, L., Palmer, P. I., Blavier, J.-F. L., Deutscher, N. M.,
2 Macatangay, R., Notholt, J., Roehl, C., Warneke, T., and Wunch, D.: Atmospheric
3 carbon dioxide retrieved from the Greenhouse gases Observing SATellite (GOSAT):
4 Comparison with ground-based TCCON observations and GEOS-Chem model
5 calculations, *J. Geophys. Res. Atmos.*, 117, D21301, doi:10.1029/2012JD018087, 2012.
- 6 Crisp, D., Atlas, R. M., Bréon, F.-M., Brown, L. R., Burrows, J. P., Ciais, P., Connor, B. J., Doney,
7 S. C., Fung, I. Y., Jacob, D. J., Miller, C. E., O'Brien, D., Pawson, S., Randerson, J. T.,
8 Rayner, P., Salawitch, R. S., Sander, S. P., Sen, B., Stephens, G. L., Tans, P. P., Toon, G.
9 C., Wennberg, P. O., Wofsy, S. C., Yung, Y. L., Kuang, Z., Chudasama, B., Sprague, G.,
10 Weiss, P., Pollock, R., Kenyon, D., and Schroll, S.: The Orbiting Carbon Observatory
11 (OCO) mission, *Adv. Space Res.*, 34, 700–709, 2004.
- 12 Deutscher, N. M., Griffith, D. W. T., Bryant, G. W., Wennberg, P. O., Toon, G. C.,
13 Washenfelder, R. A., Keppel-Aleks, G., Wunch, D., Yavin, Y., Allen, N. T., Blavier, J.-F.,
14 Jiménez, R., Daube, B. C., Bright, A. V., Matross, D. M., Wofsy, S. C., and Park, S.: Total
15 column CO₂ measurements at Darwin, Australia-site description and calibration against
16 in situ aircraft profiles, *Atmos. Meas. Tech.*, 3, 947–958, doi:10.5194/amt-3-947-2010,
17 2010.
- 18 Gatti, L. V., Miller, J. B., D'Amelio, M. T. S., Martinewski, A., Basso, L. S., Gloor, M. E., Wofsy,
19 S., and Tans, P.: Vertical profiles of CO₂ above eastern Amazonia suggest a net carbon
20 flux to the atmosphere and balanced biosphere between 2000 and 2009, *Tellus B*, 62,
21 581–594, doi:10.1111/j.1600-0889.2010.00484.x, 2010.
- 22 Geibel, M. C., Gerbig, C., and Feist, D. G.: A new fully automated FTIR system for total
23 column measurements of greenhouse gases, *Atmos. Meas. Tech.*, 3, 1363–1375,
24 doi:10.5194/amt-3-1363-2010, 2010.
- 25 Guerlet, S., Butz, A., Schepers, D., Basu, S., Hasekamp, O. P., Kuze, A., Yokota, T., Blavier, J.-
26 F., Deutscher, N. M., Griffith, D. W., Hase, F., Kyro, E., Morino, I., Sherlock, V.,
27 Sussmann, R., Galli, A., and Aben, I.: Impact of aerosol and thin cirrus on retrieving and
28 validating XCO₂ from GOSAT shortwave infrared measurements, *J. Geophys. Res.*
29 *Atmos.*, 118, 4887–4905, 2013.
- 30 Inoue, M., Morino, I., Uchino, O., Miyamoto, Y., Yoshida, Y., Yokota, T., Machida, T., Sawa, Y.,
31 Matsueda, H., Sweeney, C., Tans, P. P., Andrews, A. E., Biraud, S. C., Tanaka, T.,
32 Kawakami, S., and Patra, P. K.: Validation of XCO₂ derived from SWIR spectra of GOSAT
33 TANSO-FTS with aircraft measurement data, *Atmos. Chem. Phys.*, 13, 9771–9788,
34 doi:10.5194/acp-13-9771-2013, 2013.
- 35 Ito, A.: Changing ecophysiological processes and carbon budget in East Asian ecosystems
36 under near-future changes in climate: Implications for long-term monitoring from a
37 process-based model, *J. Plant Res.*, 123, 577–588, 2010.
- 38 Keppel-Aleks, G., Wennberg, P. O., and Schneider, T.: Sources of variations in total column
39 carbon dioxide, *Atmos. Chem. Phys.*, 11, 3581–3593, doi:10.5194/acp-11-3581-2011,
40 2011.
- 41 Keppel-Aleks, G., Wennberg, P. O., Washenfelder, R. A., Wunch, D., Schneider, T., Toon, G.
42 C., Andres, R. J., Blavier, J.-F., Connor, B., Davis, K. J., Desai, A. R., Messerschmidt, J.,
43 Notholt, J., Roehl, C. M., Sherlock, V., Stephens, B. B., Vay, S. A., and Wofsy, S. C.: The



- 1 imprint of surface fluxes and transport on variations in total column carbon dioxide,
2 Biogeosciences, 9, 875–891, doi:10.5194/bg-9-875-2012, 2012.
- 3 Kuze, A., Suto H., Nakajima M., and Hamazaki, T.: Thermal and near infrared sensor for
4 carbon observation Fourier-transform spectrometer on the Greenhouse Gases
5 Observing Satellite for greenhouse gases monitoring, Appl. Opt., 48, 6716–6733,
6 doi:10.1364/AO.48.006716, 2009.
- 7 Kuze, A., suto, H., Shiomi, K., Kawakami, S., Tanaka, M., Ueda, Y., Deguchi, A., Yoshida, J.,
8 Yamamoto, Y., Kataoka, F., Taylor, T. E., and Buijs, H.: Update on GOSAT TANSO-FTS
9 performance, operations, and data products after more than six years in space, Atmos.
10 Meas. Tech. Discuss., doi:10.5194/amt-2015-333, in review, 2016.
- 11 Lindqvist, H., O'Dell, C. W., Basu, S., Boesch, H., Chevallier, F., Deutscher, N., Feng, L., Fisher,
12 B., Hase, F., Inoue, M., Kivi, R., Morino, I., Palmer, P. I., Parker, R., Schneider, M.,
13 Sussmann, R., and Yoshida, Y.: Does GOSAT capture the true seasonal cycle of XCO₂?,
14 Atmos. Chem. Phys. Discuss., 15, 16461–16503, doi:10.5194/acpd-15-16461-2015,
15 2015.
- 16 Messerschmidt, J., Macatangay, R., Notholt, J., Petri, C., Warneke, T., and Weinzierl, C.: Side
17 by side measurements of CO₂ by ground-based Fourier transform spectrometry (FTS),
18 Tellus B, 62, 749–758, doi:10.1111/j.1600-0889.2010.00491.x, 2010.
- 19 Messerschmidt, J., Chen, H., Deutscher, N. M., Gerbig, C., Grupe, P., Katrynski, K., Koch, F.-T.,
20 Lavrič, J. V., Notholt, J., Rödenbeck, C., Ruhe, W., Warneke, T., and Weinzierl, C.:
21 Automated ground-based remote sensing measurements of greenhouse gases at the
22 Białystok site in comparison with collocated in situ measurements and model data,
23 Atmos. Chem. Phys., 12, 6741–6755, doi:10.5194/acp-12-6741-2012, 2012.
- 24 Nguyen, H., Osterman, G., Wunch, D., O'Dell, C., Mandrake, L., Wennberg, P., Fisher, B., and
25 Castano, R.: A method for collocating satellite XCO₂ data to ground-based data and its
26 application to ACOS-GOSAT and TCCON, Atmos. Meas. Tech., 7, 2631–2644,
27 doi:10.5194/amt-7-2631-2014, 2014.
- 28 Oda, T. and Maksyutov, S.: A very high-resolution (1 km × 1 km) global fossil fuel CO₂
29 emission inventory derived using a point source database and satellite observations of
30 nighttime lights, Atmos. Chem. Phys., 11, 543–556, doi:10.5194/acp-11-543-2011,
31 2011.
- 32 O'Dell, C. W., Connor, B., Bösch, H., O'Brien, D., Frankenberg, C., Castano, R., Christi, M.,
33 Eldering, D., Fisher, B., Gunson, M., McDuffie, J., Miller, C. E., Natraj, V., Oyafuso, F.,
34 Polonsky, I., Smyth, M., Taylor, T., Toon, G. C., Wennberg, P. O., and Wunch, D.: The
35 ACOS CO₂ retrieval algorithm – Part 1: Description and validation against synthetic
36 observations, Atmos. Meas. Tech., 5, 99–121, doi:10.5194/amt-5-99-2012, 2012.
- 37 Ohyama, H., Morino, I., Nagahama, T., Machida, T., Suto, H., Oguma, H., Sawa, Y., Matsueda,
38 H., Sugimoto, N., Nakane, H., and Nakagawa, K.: Column-averaged volume mixing ratio
39 of CO₂ measured with ground-based Fourier transform spectrometer at Tsukuba, J.
40 Geophys. Res., 114, D18303, doi:10.1029/2008JD011465, 2009.
- 41 Onogi, K., Tsutsui, J., Koide, H., Sakamoto, M., Kobayashi, S., Hatsushika, H., Matsumoto, T.,
42 Yamazaki, N., Kamahori, H., Takahashi, K., Kadokura, S., Wada, K., Kato, K., Oyama, R.,



- 1 Ose, T., Mannoji, N., and Taira, R.: The JRA-25 Reanalysis, *J. Meteor. Soc. Japan*, 85,
2 369–432, 2007.
- 3 Oshchepkov, S., Bril, A., Yokota, T., Morino, I., Yoshida, Y., Matsunaga, T., Belikov, D., Wunch,
4 D., Wennberg, P. O., Toon, G. C., O'Dell, C. W., Butz, A., Guerlet, S., Cogan, A., Boesch,
5 H., Eguchi, N., Deutscher, N. M., Griffith, D., Macatangay, R., Notholt, J., Sussmann, R.,
6 Rettinger, M., Sherlock, V., Robinson, J., Kyrö, E., Heikkinen, P., Feist, D. G., Nagahama,
7 T., Kadyrov, N., Maksyutov, S., Uchino, O., and Watanabe, H.: Effects of atmospheric
8 light scattering on spectroscopic observations of greenhouse gases from space:
9 Validation of PPDF-based CO₂ retrievals from GOSAT, *J. Geophys. Res.*, 117, 1–18,
10 2012.
- 11 Oshchepkov, S., Bril, A., Yokota, T., Yoshida, Y., Blumenstock, T., Deutscher, N. M., Dohe, S.,
12 Macatangay, R., Morino, I., Notholt, J., Rettinger, M., Petri, C., Schneider, M., Sussman,
13 R., Uchino, O., Velazco, V., Wunch, D., and Belikov, D.: Simultaneous retrieval of
14 atmospheric CO₂ and light path modification from space-based spectroscopic
15 observations of greenhouse gases: methodology and application to GOSAT
16 measurements over TCCON sites, *Appl. Optics*, 52, 1339–1350, 2013.
- 17 Patra, P. K., Houweling, S., Krol, M., Bousquet, P., Belikov, D., Bergmann, D., Bian, H.,
18 Cameron-Smith, P., Chipperfield, M. P., Corbin, K., Fortems-Cheiney, A., Fraser, A.,
19 Gloor, E., Hess, P., Ito, A., Kawa, S. R., Law, R. M., Loh, Z., Maksyutov, S., Meng, L.,
20 Palmer, P. I., Prinn, R. G., Rigby, M., Saito, R., and Wilson, C.: TransCom model
21 simulations of CH₄ and related species: linking transport, surface flux and chemical loss
22 with CH₄ variability in the troposphere and lower stratosphere, *Atmos. Chem. Phys.*,
23 11, 12813–12837, doi:10.5194/acp-11-12813-2011, 2011.
- 24 Reuter, M., Bösch, H., Bovensmann, H., Bril, A., Buchwitz, M., Butz, A., Burrows, J. P., O'Dell,
25 C. W., Guerlet, S., Hasekamp, O., Heymann, J., Kikuchi, N., Oshchepkov, S., Parker, R.,
26 Pfeifer, S., Schneising, O., Yokota, T., and Yoshida, Y.: A joint effort to deliver satellite
27 retrieved atmospheric CO₂ concentrations for surface flux inversions: the ensemble
28 median algorithm EMMA, *Atmos. Chem. Phys.*, 13, 1771–1780, doi:10.5194/acp-13-
29 1771-2013, 2013.
- 30 Stohl, A., Seibert, P., Arduini, J., Eckhardt, S., Fraser, P., Grealley, B. R., Lunder, C., Maione, M.,
31 Mhle, J., O'Doherty, S., Prinn, R. G., Reimann, S., Saito, T., Schmidbauer, N., Simmonds,
32 P. G., Vollmer, M. K., Weiss, R. F., and Yokouchi, Y.: An analytical inversion method for
33 determining regional and global emissions of greenhouse gases: Sensitivity studies and
34 application to halocarbons, *Atmos. Chem. Phys.*, 9, 1597–1620, doi:10.5194/acp-9-
35 1597-2009, 2009.
- 36 Swap, R., Garstang, M., Macko, S. A., Tyson, P. D., Maenhaut, W., Artaxo, P., Källberg, P., and
37 Talbot R.: The long-range transport of southern African aerosols to the tropical South
38 Atlantic, *J. Geophys. Res.*, 101(D19), 23777–23791, doi:10.1029/95JD01049, 1996.
- 39 Valsala, V., and Maksyutov, S.: Interannual variability of the air–sea CO₂ flux in the north
40 Indian Ocean, *Ocean Dynam.*, 63, 165–178, doi:10.1007/s10236-012-0588-7, 2013.
- 41 Van der Werf, G. R., Randerson, J. T., Giglio, L., Collatz, G. J., Mu, M., Kasibhatla, P. S.,
42 Morton, D. C., DeFries, R. S., Jin, Y., and Van Leeuwen, T. T.: Global fire emissions and



1 the contribution of deforestation, savanna, forest, agricultural, and peat fires (1997–
2 2009), *Atmos. Chem. Phys.*, 10, 11707–11735, doi:10.5194/acp-10-11707-2010, 2010.
3 Washenfelder, R., Toon, G., Blavier, J., Yang, Z., Allen, N., Wennberg, P., Vay, S., Matross, D.,
4 and Daube, B.: Carbon dioxide column abundances at the Wisconsin Tall Tower site, *J.*
5 *Geophys. Res.*, 111, D22305, doi:10.1029/2006JD007154, 2006.
6 Wunch D., Toon, G.C., Blavier, J.-F.L., Washenfelder, R.A., Notholt, J., Connor, B.J., Griffith,
7 D.W.T., Sherlock, V., and Wennberg, P.O.: The Total Carbon Column Observing
8 Network, *Phil. Trans. R. Soc. A* 369, 2087–2112, doi:10.1098/rsta.2010.0240, 2011.
9 Yokota, T., Yoshida, Y., Eguchi, N., Ota, Y., Tanaka, T., Watanabe, H., and Maksyutov, S.:
10 Global concentrations of CO₂ and CH₄ retrieved from GOSAT: First preliminary results,
11 *SOLA*, 5, 160–163, doi:10.2151/sola.2009-041, 2009.
12 Yoshida, Y., Kikuchi, N., Morino, I., Uchino, O., Oshchepkov, S., Bril, A., Saeki, T., Schutgens,
13 N., Toon, G. C., Wunch, D., Roehl, C. M., Wennberg, P. O., Griffith, D. W. T., Deutscher,
14 N. M., Warneke, T., Notholt, J., Robinson, J., Sherlock, V., Connor, B., Rettinger, M.,
15 Sussmann, R., Ahonen, P., Heikkinen, P., Kyrö, E., Mendonca, J., Strong, K., Hase, F.,
16 Dohe, S., and Yokota, T.: Improvement of the retrieval algorithm for GOSAT SWIR XCO₂
17 and XCH₄ and their validation using TCCON data, *Atmos. Meas. Tech.*, 6, 1533–1547,
18 doi:10.5194/amt-6-1533-2013, 2013.
19 Zhuravlev, R.V., Ganshin, A.V., Maksyutov, S.S., Oshchepkov, S.L., Khattatov, B.V.: Estimation
20 of global fluxes of CO₂ using ground-station and satellite (GOSAT) observation data
21 with empirical orthogonal functions. *Atmos. Oceanic Opt.*, 26, 388-397, 2013.
22



1 **Table 1.** Details of operational TCCON sites.

Number	Site	Latitude (Degrees)	Longitude (Degrees)	Altitude (km)
1	Anmyeondo, Korea	36.54	126.33	0.03
2	Ascension Island	7.92	-14.33	0.03
3	Białystok, Poland	53.23	23.03	0.18
4	Bremen, Germany	53.10	8.85	0.03
5	Caltech, USA	34.14	-118.13	0.23
6	Darwin, Australia	-12.42	130.89	0.03
7	Edwards, USA	34.96	-117.88	0.70
8	Eureka, Canada	80.05	-86.42	0.61
9	Garmisch, Germany	47.48	11.06	0.74
10	Izaña, Tenerife	28.30	-16.50	2.37
11	Karlsruhe, Germany	49.10	8.44	0.12
12	Lamont, USA	36.60	-97.49	0.32
13	Lauder, New Zealand	-45.04	169.68	0.37
14	Ny Ålesund, Spitsbergen	78.90	11.90	0.02
15	Orléans, France	47.97	2.11	0.13
16	Park Falls, USA	45.95	-90.27	0.44
17	Paris, France	48.85	2.32	0.10
18	La Réunion Island, France	-20.90	55.49	0.09
19	Rikubetsu, Japan	43.46	143.77	0.36
20	Saga, Japan	33.24	130.29	0.01
21	Sodankylä, Finland	67.37	26.63	0.19
22	Tsukuba, Japan	36.05	140.12	0.03
23	Wollongong, Australia	-34.41	150.88	0.03

2

3 **Table 2.** Past, future, and possible TCCON sites.

Number	Site	Latitude (Degrees)	Longitude (Degrees)	Altitude (km)
1	Arrival Heights, Antarctica	-77.83	166.66	0.25
2	Burgos, Philippines	18.50	120.85	0.10
3	East Trout Lake, Canada	54.35	-104.98	0.49
4	Four Corners, USA	36.80	-108.48	1.64
5	Manaus, Brazil	-3.10	-60.02	0.09
6	Oxfordshire, UK	51.57	-1.32	0.07
7	Paramaribo, Suriname	5.80	-55.20	0.05
8	Poker Flat, USA	65.12	-147.47	0.21
9	Yekaterinburg, Russia	57.04	59.55	0.30

4



1 **Table 3.** Averaged results of different collocation methods implemented for XCO₂ from NIES TM
 2 calculated for 16 TCCON sites. *The number of FLEXPART cells with resolution 1.0° × 1.0° is counted
 3 for methods based on the footprint (1–4), while for other methods NIES TM cells (2.5° × 2.5°) are
 4 used.

Case	Method of collocation	Mean number of cells*	Mean correlation coefficient	Absolute value of mean bias	Mean standard deviation
C1	Footprint limit $\log_{10}(x) = -0.5$	35	0.96	0.75	1.01
C2	Footprint limit $\log_{10}(x) = -1.0$	160	0.96	0.81	0.98
C3	Footprint limit $\log_{10}(x) = -1.5$	507	0.97	0.85	0.97
C4	Footprint limit $\log_{10}(x) = -2.0$	1071	0.97	0.88	0.96
C5	Within area of 2.5° × 2.5°	1	0.96	0.76	1.03
C6	Within area of ±5.0° × ±5.0°	16	0.96	0.79	1.00
C7	Within area of ±5.0° × ±10.0°	32	0.96	0.79	0.98
C8	Within area of ±7.5° × ±22.5°	108	0.97	0.80	0.97

5

6 **Table 4.** Averaged results of different collocation methods implemented for XCO₂ from the GOSAT
 7 ACOS product calculated for 16 TCCON sites.

Case	Method of collocation	Mean number of observations	Mean correlation coefficient	Absolute value of mean bias	Mean standard deviation
C1	Footprint limit $\log_{10}(x) = -0.5$	1190	0.93	0.65	1.18
C2	Footprint limit $\log_{10}(x) = -1.0$	3046	0.92	0.61	1.21
C3	Footprint limit $\log_{10}(x) = -1.5$	4880	0.93	0.62	1.15
C4	Footprint limit $\log_{10}(x) = -2.0$	6016	0.93	0.64	1.12
C5	Within area of 2.5° × 2.5°	976	0.93	0.81	1.11
C6	Within area of ±5.0° × ±5.0°	2042	0.92	0.67	1.19
C7	Within area of ±5.0° × ±10.0°	3111	0.92	0.65	1.19
C8	Within area of ±7.5° × ±22.5°	5002	0.93	0.64	1.16

8

9



1 **Table 5.** Averaged results of different collocation methods implemented for XCO₂ from the GOSAT
 2 NIES product calculated for 16 TCCON sites.

Case	Method of collocation	Mean number of observations	Mean correlation coefficient	Absolute value of mean bias	Mean standard deviation
C1	Footprint limit $\log_{10}(x) = -0.5$	1049	0.89	0.63	1.14
C2	Footprint limit $\log_{10}(x) = -1.0$	2890	0.92	0.52	1.20
C3	Footprint limit $\log_{10}(x) = -1.5$	4823	0.92	0.60	1.19
C4	Footprint limit $\log_{10}(x) = -2.0$	5922	0.92	0.56	1.16
C5	Within area of $2.5^\circ \times 2.5^\circ$	907	0.89	0.63	1.17
C6	Within area of $\pm 5.0^\circ \times \pm 5.0^\circ$	1845	0.91	0.56	1.15
C7	Within area of $\pm 5.0^\circ \times \pm 10.0^\circ$	2976	0.93	0.58	1.15
C8	Within area of $\pm 7.5^\circ \times \pm 22.5^\circ$	4874	0.92	0.60	1.17

3

4 **Table 6.** Averaged results of different collocation methods implemented for XCO₂ from the GOSAT
 5 PPDF product calculated for 16 TCCON sites.

Case	Method of collocation	Mean number of observations	Mean correlation coefficient	Absolute value of mean bias	Mean standard deviation
C1	Footprint limit $\log_{10}(x) = -0.5$	357	0.84	0.50	1.11
C2	Footprint limit $\log_{10}(x) = -1.0$	870	0.86	0.62	1.12
C3	Footprint limit $\log_{10}(x) = -1.5$	1536	0.81	0.73	1.16
C4	Footprint limit $\log_{10}(x) = -2.0$	1911	0.81	0.67	1.17
C5	Within area of $2.5^\circ \times 2.5^\circ$	331	0.86	0.66	1.02
C6	Within area of $\pm 5.0^\circ \times \pm 5.0^\circ$	749	0.85	0.64	1.15
C7	Within area of $\pm 5.0^\circ \times \pm 10.0^\circ$	1114	0.83	0.69	1.19
C8	Within area of $\pm 7.5^\circ \times \pm 22.5^\circ$	1733	0.86	0.68	1.17

6

7 **Table 7.** Averaged results of different collocation methods implemented for XCO₂ from the GOSAT
 8 RemoTeC product calculated for 16 TCCON sites.

Case	Method of collocation	Mean number of observations	Mean correlation coefficient	Absolute value of mean bias	Mean standard deviation
C1	Footprint limit $\log_{10}(x) = -0.5$	795	0.81	0.71	1.17
C2	Footprint limit $\log_{10}(x) = -1.0$	1898	0.83	0.66	1.19
C3	Footprint limit $\log_{10}(x) = -1.5$	3212	0.83	0.61	1.22
C4	Footprint limit $\log_{10}(x) = -2.0$	4091	0.83	0.59	1.21
C5	Within area of $2.5^\circ \times 2.5^\circ$	769	0.90	0.87	1.15
C6	Within area of $\pm 5.0^\circ \times \pm 5.0^\circ$	1491	0.85	0.63	1.18
C7	Within area of $\pm 5.0^\circ \times \pm 10.0^\circ$	2325	0.86	0.70	1.19
C8	Within area of $\pm 7.5^\circ \times \pm 22.5^\circ$	3818	0.86	0.64	1.25



1 **Table 8.** Averaged results of different colocation methods implemented for XCO₂ from the GOSAT
 2 UoL-FP product calculated for 16 TCCON sites.

Case	Method of colocation	Mean number of observations	Mean correlation coefficient	Absolute value of mean bias	Mean standard deviation
C1	Footprint limit $\log_{10}(x) = -0.5$	634	0.88	0.78	1.31
C2	Footprint limit $\log_{10}(x) = -1.0$	1454	0.87	0.76	1.34
C3	Footprint limit $\log_{10}(x) = -1.5$	2450	0.88	0.80	1.28
C4	Footprint limit $\log_{10}(x) = -2.0$	3017	0.89	0.70	1.23
C5	Within area of $2.5^\circ \times 2.5^\circ$	629	0.86	0.73	1.33
C6	Within area of $\pm 5.0^\circ \times \pm 5.0^\circ$	1215	0.88	0.76	1.30
C7	Within area of $\pm 5.0^\circ \times \pm 10.0^\circ$	1852	0.86	0.74	1.27
C8	Within area of $\pm 7.5^\circ \times \pm 22.5^\circ$	2799	0.85	0.72	1.25

3

4 **Table 9.** Comparison of colocation methods C4 versus C8 using ACOS, NIES, PPDF, RemoTeC, and
 5 UoL GOSAT products near the Darwin site.

GOSAT Product	Case	Correlation coefficient	Mean bias	Standard deviation	Number of observations
ACOS	C4	0.96	0.36	0.77	36292
	C8	0.94	0.50	0.90	10872
NIES	C4	0.94	0.09	0.88	26652
	C8	0.93	0.13	1.00	6924
PPDF	C4	0.70	0.24	1.02	13681
	C8	0.64	0.08	1.10	4333
RemoTeC	C4	0.91	0.44	0.95	23915
	C8	0.89	0.77	1.07	7130
UoL	C4	0.82	0.34	1.17	14376
	C8	0.86	0.17	1.10	4727

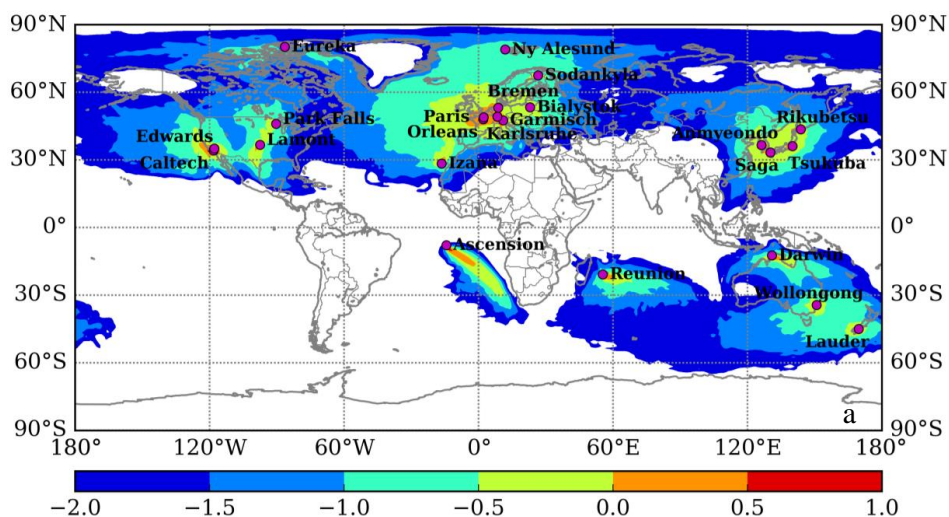
6 **Table 10.** Comparison of colocation methods C4 versus C8 using ACOS, NIES, RemoTeC, and UoL
 7 GOSAT products near the La Réunion site. The PPDF GOSAT product does not include any
 8 observations near the La Réunion site.

GOSAT Product	Case	Correlation coefficient	Mean bias	Standard deviation	Number of observations
ACOS	C4	0.82	0.70	0.83	11873
	C8	0.83	0.65	0.76	9640
NIES	C4	0.70	0.25	1.07	7720
	C8	0.73	0.45	1.02	6505
RemoTeC	C4	0.51	0.92	1.07	2482
	C8	0.61	1.16	1.04	3414
UoL	C4	0.45	0.75	0.94	860
	C8	0.36	0.71	1.00	2239

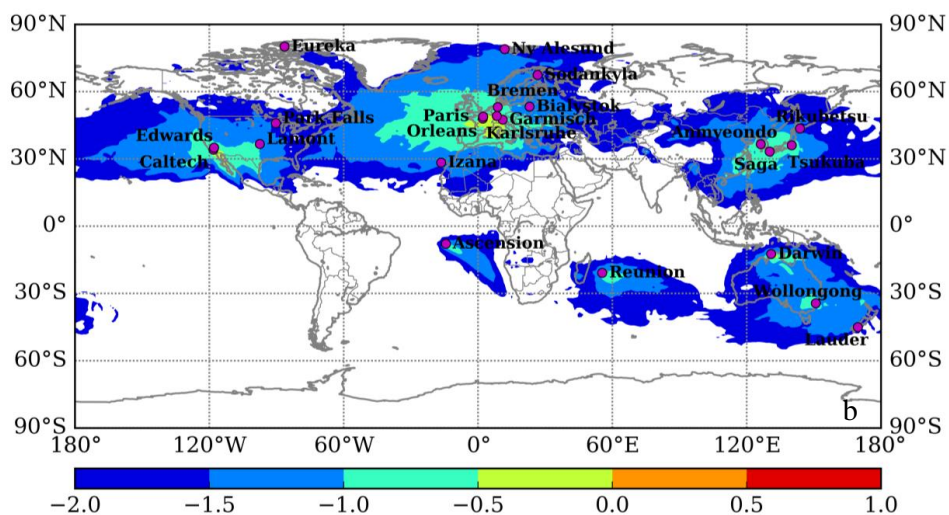
9



1

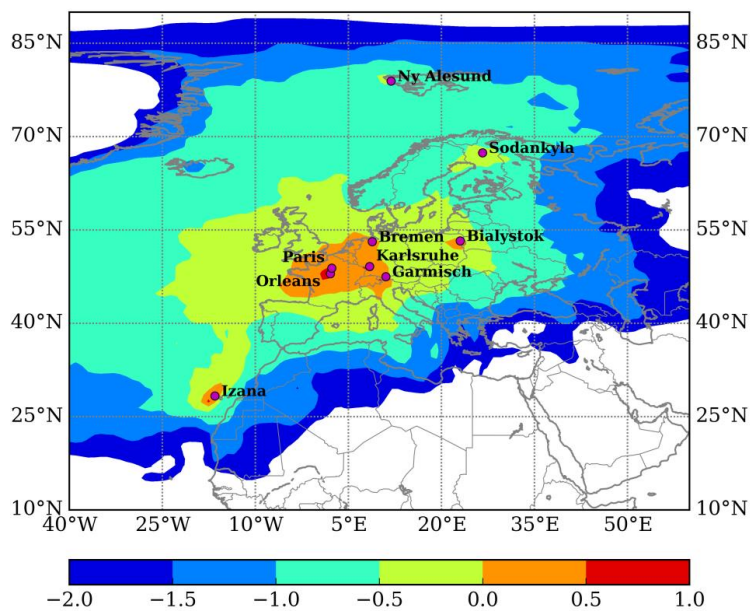


2



3

4 **Fig. 1.** Global distribution of the sensitivity of CO₂ concentrations (ppm (μmol (m²s)⁻¹)⁻¹) with
5 respect to the concentrations in adjacent cells, calculated using the FLEXPART model with a
6 resolution of 1.0° for the 23 TCCON operational sites: a) tracer simulation initialized at the
7 level of 1000 m, b) tracer simulation initialized at the level of 3000 m that corresponds to
8 700 hPa based on the International Standard Atmosphere for dry air.
9

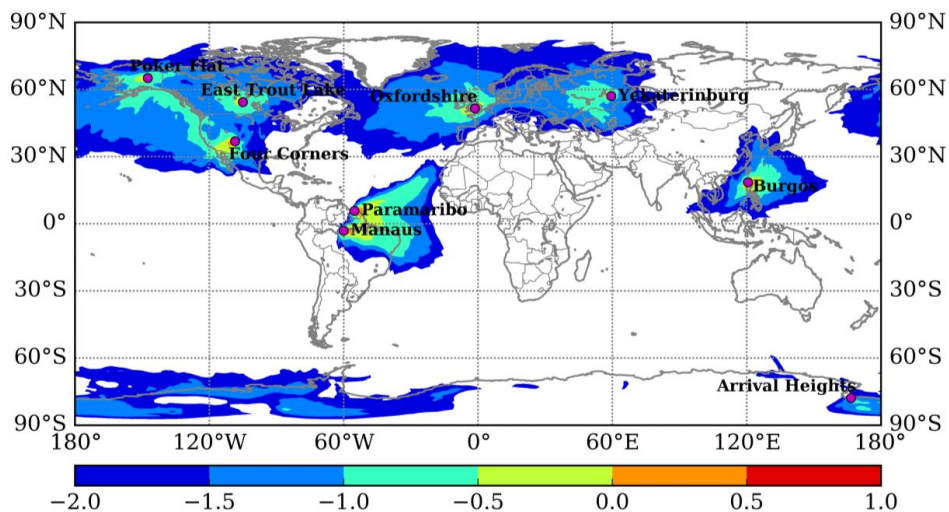


1

2 **Fig. 2.** Distribution of the sensitivity of CO₂ concentrations (ppm (μmol (m²s)⁻¹)⁻¹) in Europe with
3 respect to the concentrations in adjacent cells, calculated using the FLEXPART model with a
4 resolution of 1.0° for TCCON operational sites within Europe, using a tracer simulation
5 initialized at the level of 1000 m.
6



1



2

3 **Fig. 3.** Global distribution of the sensitivity of CO₂ concentrations (ppm (μmol (m²s)⁻¹)⁻¹) with
4 respect to the concentrations in adjacent cells, calculated using the FLEXPART model with a
5 resolution of 1.0° for 9 past, future, and possible TCCON operational sites, using a tracer
6 simulation initialized at the level of 1000 m.
7

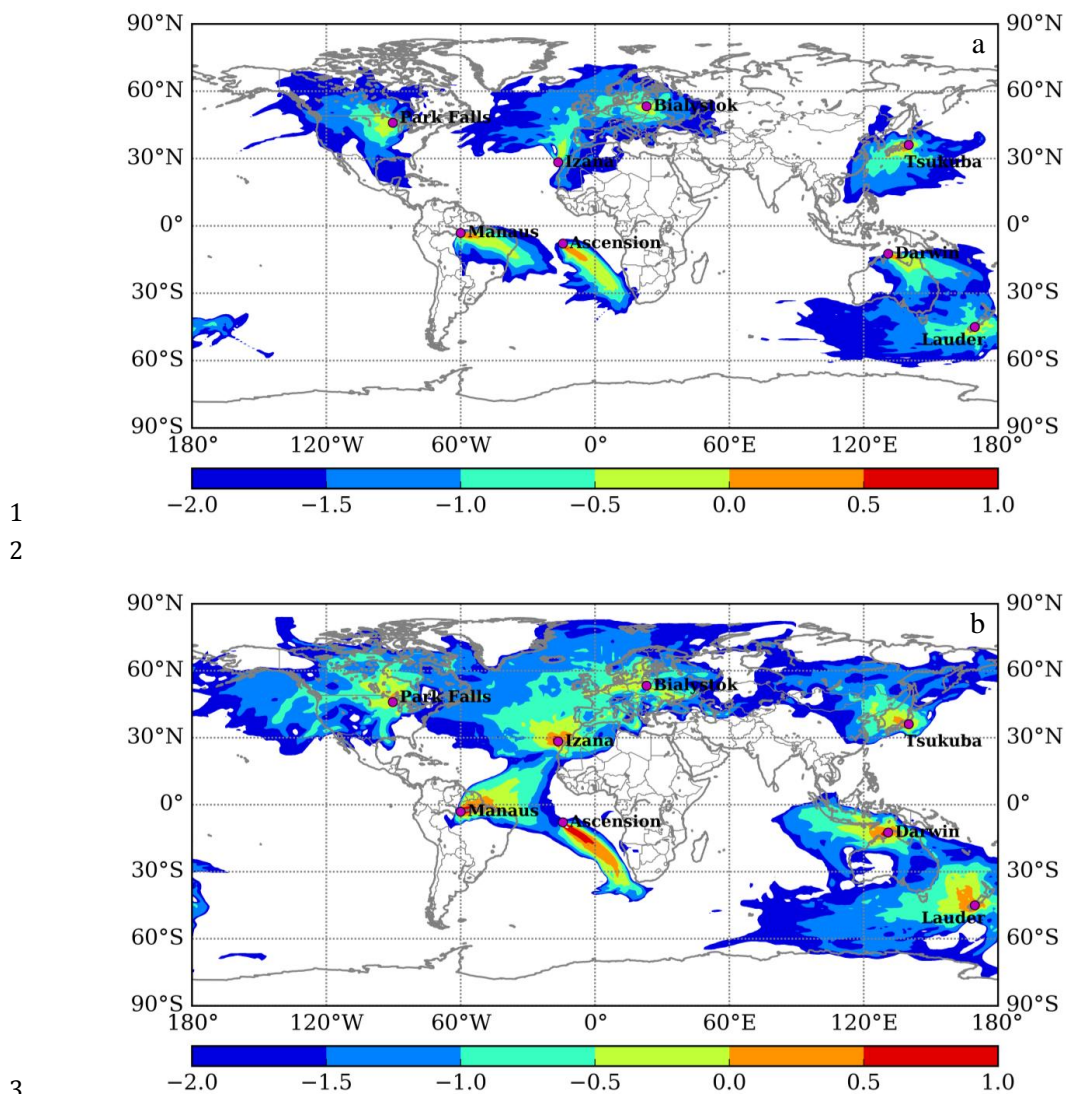
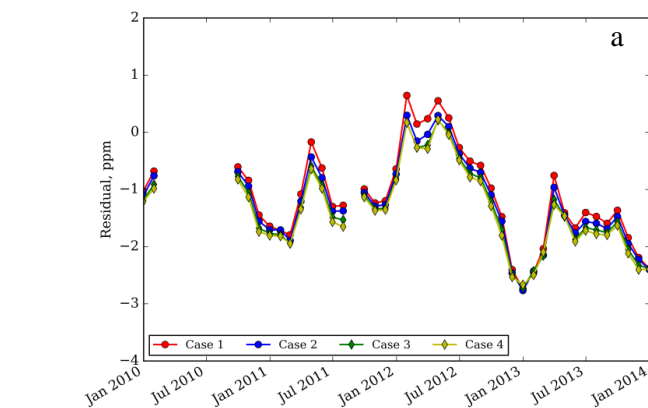
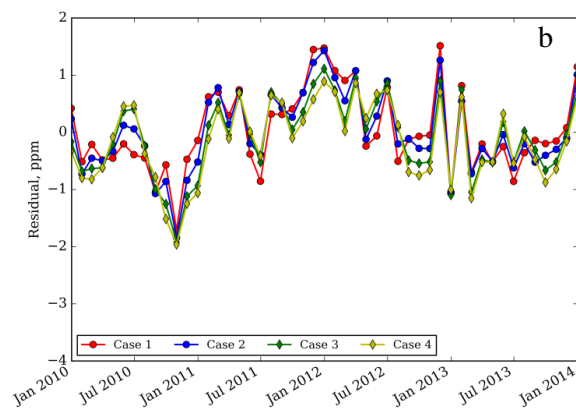


Fig. 4. Footprints for different seasons for Ascension Island, Białystok, Darwin, Izaña, Manaus, Park Falls, and Tsukuba, for a) the summer (June, July, and August) of 2010 and b) the winter (December, January, February) of 2010–2011.



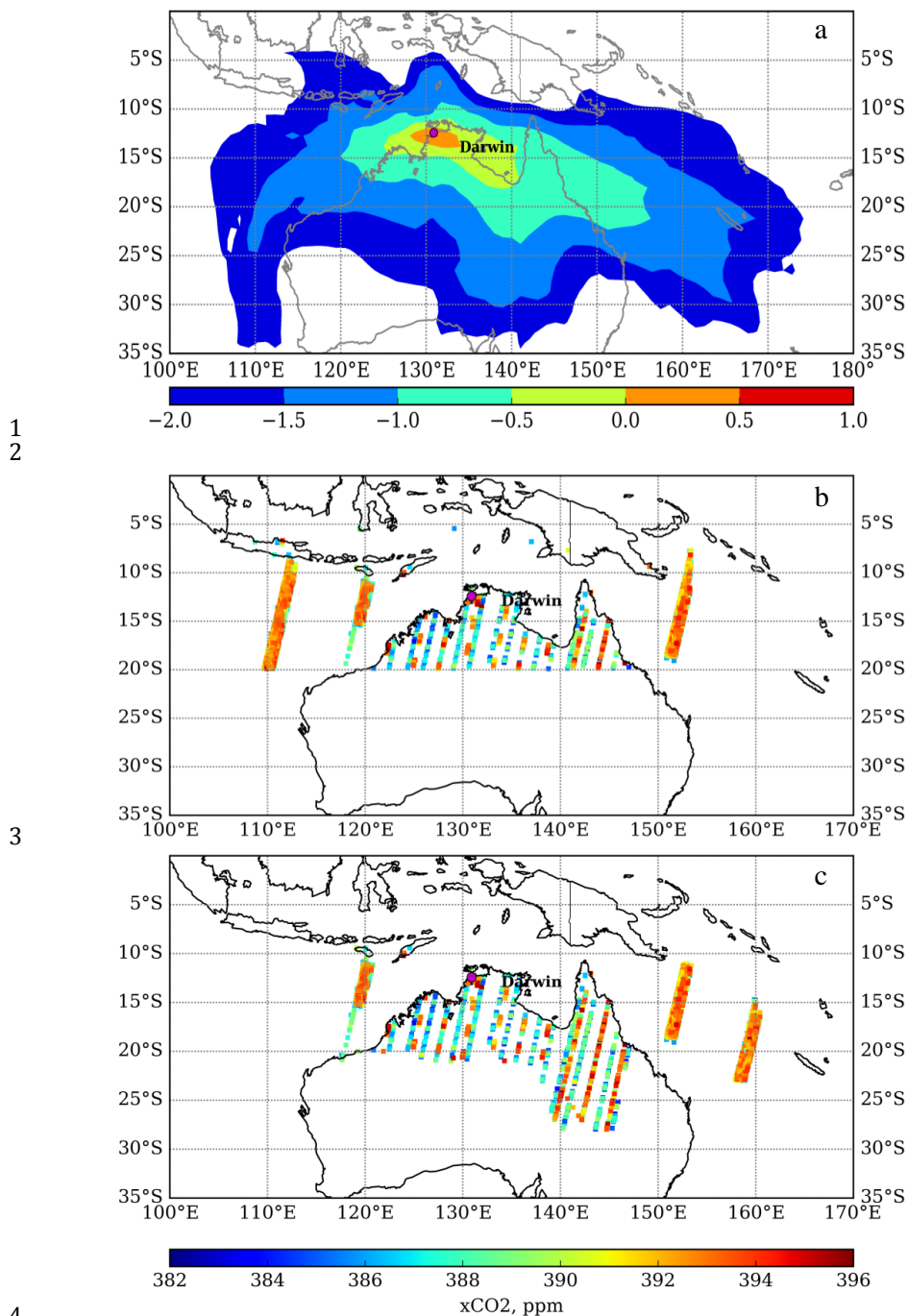
1



2

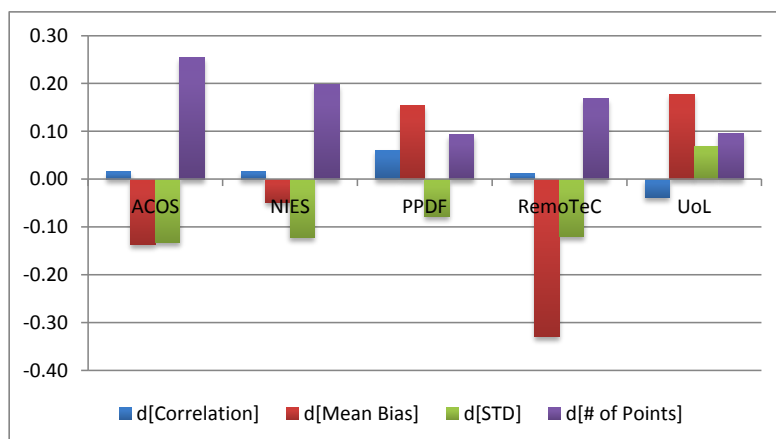
3 **Fig. 5.** Monthly average residuals of modeled XCO₂ compared with TCCON ground-based FTS for
4 methods C1, C4, C5 and C8, for a) Darwin and b) Garmisch.

5



5
6
7
8

Fig. 6. a) Annual average footprint for the Darwin TCCON observation site; ACOS GOSAT XCO₂ observations selected using b) the geostatistical method within an area of $\pm 7.5^\circ \times \pm 22.5^\circ$, and c) the footprint-based method with the limit $\log_{10}(x) = -2.0$.



1

2 **Fig. 7.** Difference (denoted as d[]) in correlation coefficients, mean bias (ppm), STD (ppm) and
3 number of observational points between methods C4 and C8 using ACOS, NIES, PPDF,
4 RemoTeC, and UoL GOSAT products near the Darwin site. Please note scale of number of
5 observational points is 10^5 .
6

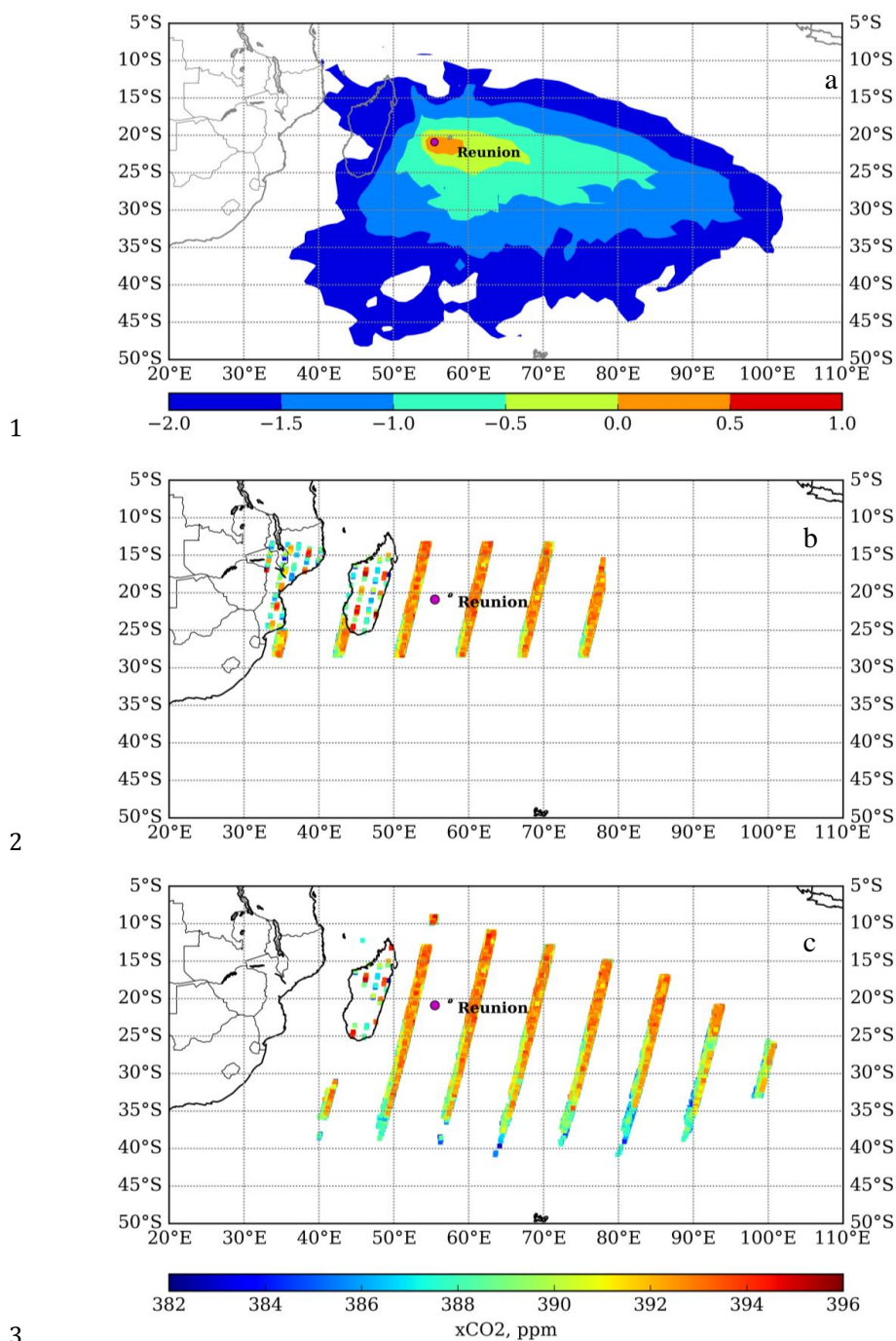
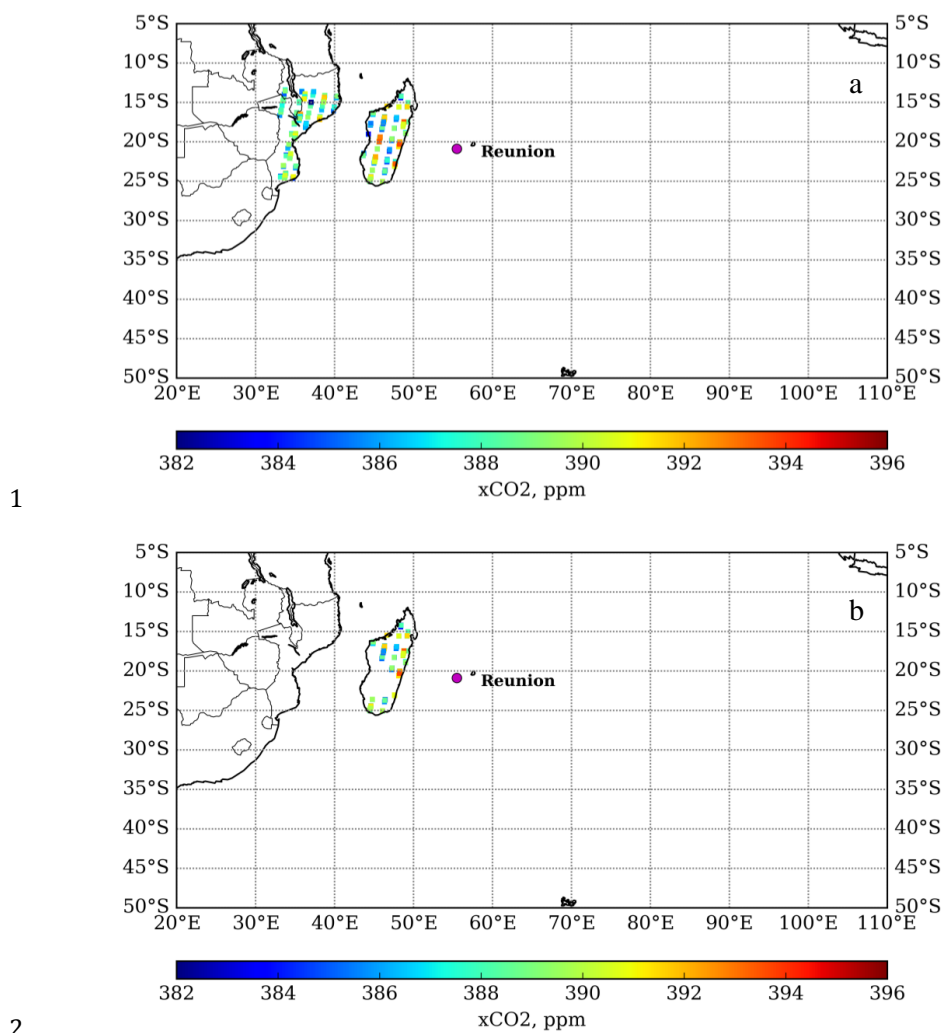
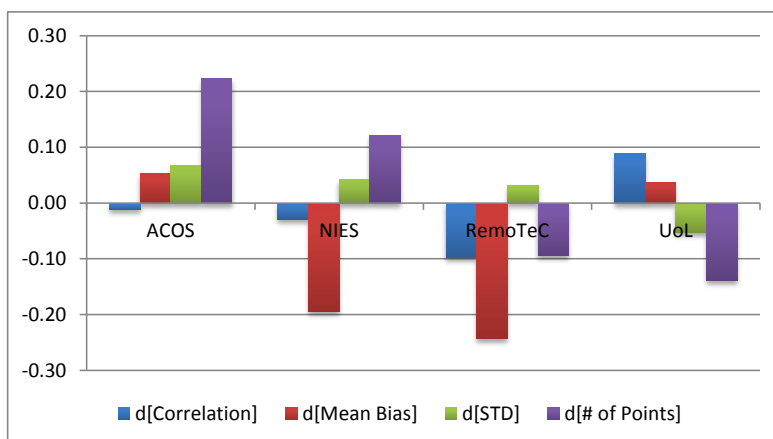


Fig. 8. a) Annual average footprint for the La Réunion TCCON observation site; ACOS GOSAT XCO₂ observations selected using b) the geostatistical method within an area of $\pm 7.5^\circ \times \pm 22.5^\circ$, and c) the footprint-based method with the limit $\log_{10}(x) = -2.0$.



3 **Fig. 9.** UoL-FP GOSAT XCO₂ observations selected using a) the geostatistical method within an
4 area of $\pm 7.5^\circ \times \pm 22.5^\circ$, and b) the footprint-based method with the limit $\log_{10}(x) = -2.0$.
5



1

2 **Fig. 10.** Difference (denoted as d[]) in correlation coefficients, mean bias (ppm), STD (ppm)
 3 and number of observational points between methods C4 and C8 using ACOS, NIES,
 4 RemoTeC, and UoL GOSAT products near the La Réunion site. Please note scale of number
 5 of observational points is 10^4 .
 6